Instability of vortex array and transitions to turbulence in rotating helium II

Makoto Tsubota,[1] Carlo F. Barenghi,[2] Tsunehiko Araki,[1] and Akira Mitani[1]
[1]*Department of Physics, Osaka City University, Sumiyoshi-Ku, Osaka 558-8585, Japan*
[2]*School of Mathematics and Statistics, University of Newcastle, Newcastle upon Tyne NE1 7RU, United Kingdom*
(Received 22 May 2003; revised manuscript received 17 February 2004; published 21 April 2004)

We consider superfluid helium inside a container which rotates at constant angular velocity and investigate numerically the stability of the array of quantized vortices in the presence of an imposed axial counterflow. This problem was studied experimentally by Swanson *et al.*, who reported evidence of instabilities at increasing axial flow but were not able to explain their nature. We find that Kelvin waves on individual vortices become unstable and grow in amplitude, until the amplitude of the waves becomes large enough that vortex reconnections take place and the vortex array is destabilized. We find that the eventual nonlinear saturation of the instability consists of a turbulent tangle of quantized vortices which is strongly polarized. The computed results compare well with the experiments. We suggest a theoretical explanation for the second instability which was observed at higher values of the axial flow and conclude by making an analogy between the alignment of vortices in the presence of rotation and the alignment of dipole moments in the presence of an applied magnetic field.

DOI: 10.1103/PhysRevB.69.134515 PACS number(s): 67.40.Vs, 47.37.+q

I. INTRODUCTION

The work described in this article is concerned with the stability of a superfluid vortex array. It is well known[1,2] that if helium II is rotated at constant angular velocity Ω, an array of superfluid vortex lines is created. The vortices are aligned along the axis of rotation and form an array with areal density given by

$$L_R = \frac{2\Omega}{\kappa}, \tag{1}$$

where $\kappa = h/m = 9.97\times 10^{-4}$ cm^2/s is the quantum of circulation, h is Plank's constant, and m the mass of one helium atom. Equation (1) is valid provided that Ω exceeds a small critical value.[3] Rotation frequencies of the order of 1 Hz are easily achieved in a laboratory, and correspond to real densities of the order of 10^3 cm^{-2}.

It is also well known that a superfluid vortex line becomes unstable in the presence of normal fluid in the direction parallel to the axis of the vortex. This instability, hereafter referred to as the Donnelly-Glaberson (DG) instability, was first observed experimentally by Cheng *et al.*[4] and then explained by Glaberson *et al.*[5] Physically, the DG instability takes the form of Kelvin waves (helical displacements of the vortex core) which grow exponentially with time.

In this paper we use an imposed axial flow to trigger the DG instability and study the transition from order to disorder in an array of quantized vortex lines. It is useful to remark here that since the growth of Kelvin waves takes place at the expense of normal fluid's energy, understanding the DG instability is also relevant[6] to the balance of energy between normal fluid and superfluid in helium II turbulence, a problem which is attracting current experimental[7–10] and theoretical[11–14] attention.

Another important meaning of this paper is to develop the formulation of three-dimensional vortex dynamics in a rotating frame. In recent years there has been a growing interest in the vortex dynamics under rotation. For example, Finne *et al.* used nuclear magnetic resonance to study the B phase of rotating superfluid ^{3}He and observed a sharp velocity-independent transition at a critical temperature between two regimes.[15] Regular behavior occurred at high temperatures, while turbulence occurred at low temperatures. They also found that the experimental results were consistent with the numerical vortex dynamics simulation that was carried out by the method described in this paper. Although the formulation of the vortex dynamics under rotation was presented briefly in our previous paper,[16] it is necessary to describe it in detail in this paper.

The paper is organized in the following way. In Sec. II we describe the rotating counterflow configuration, which is relevant to both theory and experiment. In Sec. III we summarize experimental results obtained by Swanson, Barenghi, and Donnelly.[17] They discovered that the DG mechanism can destabilize the superfluid vortex array and revealed the existence of two different superfluid turbulent states which appear if the driving axial flow exceeds the critical velocities V_{c1} and V_{c2}, respectively. Until now, the actual physical nature of these two states has been a mystery, and it is the aim of our work to shed light into this problem. In Sec. IV we set up the formulation of vortex dynamics in the rotating frame which generalizes the previous approach of Schwarz[18] and which we use in our numerical calculations. Sec. V is devoted to the first critical velocity V_{c1}, which agrees with the values predicted by the DG instability. What happens beyond V_{c1} cannot be predicted by linear stability theory and must be determined by direct nonlinear computation, which is what we do in Sec. VI. In Sec. VII we analyze the numerical results and argue that this regime $V_{c1} < V_{ns} < V_{c2}$ is a state of polarized turbulence. In Sec. VIII we speculate that the second critical velocity V_{c2} marks the onset of an unpolarized turbulent state. In Sec. IX we show an analogy between counterflow turbulence in the presence of an applied

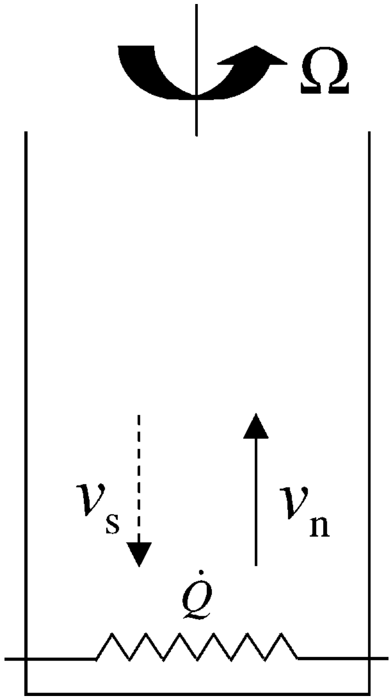

FIG. 1. Schematic rotating counterflow apparatus.

rotation and a system of spins in contact with a heat bath in the presence of an applied magnetic field. Finally Sec. X draws the conclusions.

II. ROTATING COUNTERFLOW

In order to study the stability of the rotating superfluid vortex array, we consider the configuration which is schematically shown in Fig. 1. A channel, which is closed at one end and open to the helium bath at the other end, is placed on a table which can be rotated at an assigned angular velocity Ω. At the closed end of the channel a resistor dissipates a known heat flux $\dot{Q}$.

First let us consider what happens in the absence of rotation ($\Omega=0$). Since only the normal fluid carries entropy, then $\dot{Q}=\rho TSV_n$, where T is the absolute temperature, S the specific entropy, $\rho=\rho_s+\rho_n$ the total density of helium II, ρ_s the superfluid density, and ρ_n the normal-fluid density. We call V_n and V_s, respectively, the normal-fluid and the superfluid velocity fields in the direction along the channel, averaged over the channel's cross section. The total mass flux $\rho_s V_s+\rho_n V_n$ is zero because one end of the channel is closed. The resulting counterflow velocity $V_{ns}=V_n-V_s$, which is induced along the channel is therefore proportional to the applied heat flux:

$$V_{ns}=\frac{\dot{Q}}{\rho_s ST}. \tag{2}$$

It is known from experiments[19,20] and numerical simulations[18] that, if $\dot{Q}$ (hence V_{ns}) exceeds a critical value, a turbulent tangle of quantized vortex lines is created. The tangle is homogeneous and isotropic (neglecting a small degree of anisotropy induced by the direction of the imposed heat current). The intensity of the turbulence is measured by the vortex line density (length of vortex line per unit volume) which is experimentally determined by monitoring the extra attenuation of second sound. One finds that, for $V_{ns}>V_0$, the vortex line density has the form

$$L_H=\gamma_H^2 V_{ns}^2, \tag{3}$$

where γ_H is a temperature-dependent coefficient[19] and V_0 is a small critical velocity which depends on the temperature and on the size and geometry of the channel.[19]

Let us consider now the case in which the heat flux is applied in the rotating frame ($\Omega\neq 0$). We have now two effects which compete with each other: rotation, which favors the creation of an ordered array of vortices aligned along the direction of the axis of rotation, and counterflow, which favors the creation of a disordered tangle. Swanson *et al.*[17] were the first to address the problem of whether the vortex array is stable or not at given values of Ω and V_{ns}, and, if the array is unstable, of whether the vortex line density L is the sum of Eqs. (1) and (3) or not. Their experimental results are described in the following section.

It is important to remark that, in principle, one can also study the stability of a vortex array in the presence of a mass flow rather than of a heat current. Similarly, one can study the effects of rotation upon the turbulence of helium II created by towing a grid or rotating a propeller rather than upon counterflow turbulence. The reason for which we have chosen to restrict our investigation to the case of a heat current is twofold: first, the experimental data of Swanson *et al.*[17] are available; second, at least at small heat currents,[21] the turbulent superfluid tangle is homogeneous and almost isotropic and we do not have to worry about large-scale motion and eddies of the normal fluid.

III. THE EXPERIMENT

The rotating counterflow apparatus of Swanson *et al.*[17] consisted of a 40 cm long vertical channel of $1\times 1\ \mathrm{cm}^2$ square cross section. At the closed end (as shown in Fig. 1) a resistor dissipated a known heat flux $\dot{Q}$ and induced relative motion V_{ns} of the two fluid components. The vortex line density L was measured by pairs of second sound transducers located along the channel. The entire apparatus was set up on a rotating cryostat, so that it was possible to create vortex lines by either rotation or counterflow, or by any combination of them. The vortex line density was calculated from a measurement of the attenuation of second sound resonances and its calibration against the known density in rotation.[22]

The experiment was performed at $T=1.65$ K. In the presence of both rotation and counterflow three distinct flow states were observed, as shown in Figs. 2 and 3, respectively, at high and low rotations. The three states are separated by two critical counterflow velocities V_{c1} and V_{c2} (see Fig. 2). The results of the experiment can be summarized at increasing values of V_{ns} as follows.

(1) *State* $V_0<V_{ns}<V_{c1}$. In the first region of Fig. 2 at the left of V_{c1} the vortex line density is independent of the small values of V_{ns} involved and agrees with Eq. (1). This region

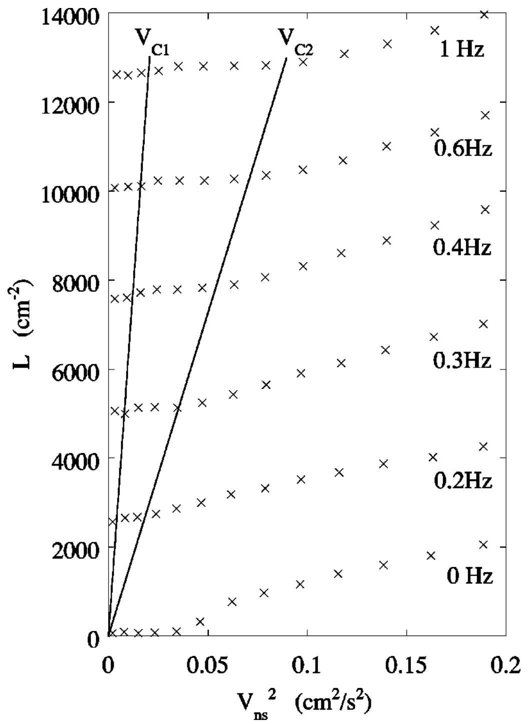

FIG. 2. Vortex line density L observed by Swanson *et al.* in the presence of a counterflow heat current V_{ns} at various rotation rates at $T=1.65$ K. The solid lines represent Swanson *et al.*'s fits to the two observed critical velocities V_{c1} and V_{c2}. The experimental uncertainties are about 1/3 of the symbol size. This data set shows the highest rotation rates to put in evidence the curves V_{c1} and V_{c2}.

clearly corresponds to an ordered vortex array, and the counterflow current V_{ns} is not strong enough to destabilize it. Note that if $\Omega \neq 0$ then $V_0=0$.

(2) *Transition at* $V_{ns}=V_{c1}$. Swanson *et al.*[17] noticed that the values of the first critical velocity V_{c1} are consistent with the DG instability. This means that at $V_{ns}=V_{c1}=V_{DG}$ the axial flow is so strong that Kelvin waves of infinitesimal amplitude become unstable and grow.

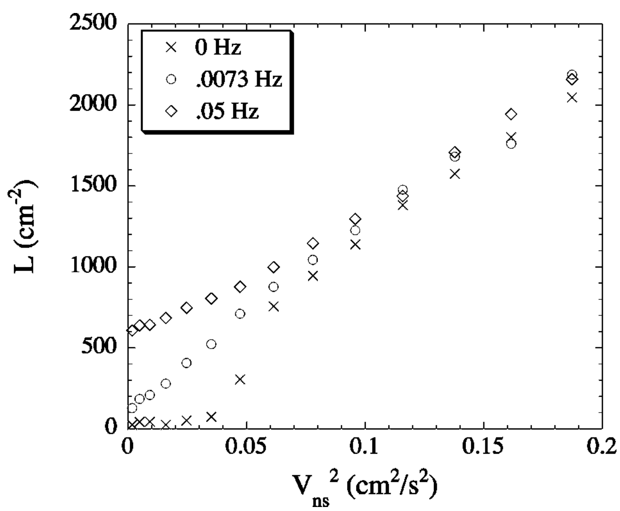

FIG. 3. Vortex line density L observed by Swanson *et al.* This data set shows the smallest counterflow velocities at the smallest rotation rates to show that the critical velocity for $\Omega=0$ disappears in the presence of rotation.

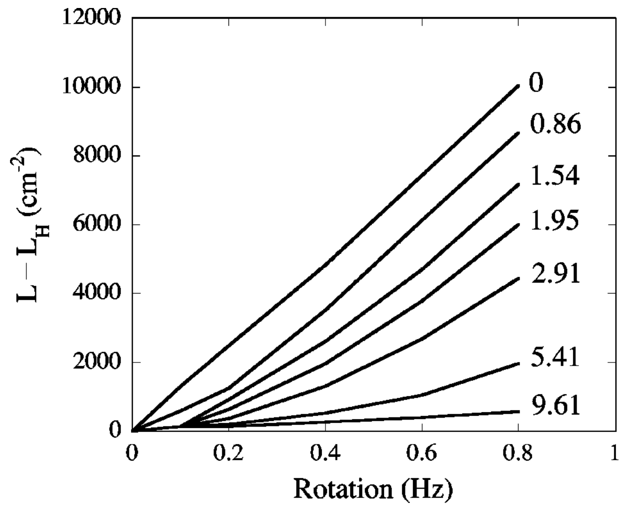

FIG. 4. Excess vortex line density with rotation $L-L_H$ vs rotation at values of V_{ns} up to the highest values, as observed by Swanson *et al.* The number near each curve is the value of V_{ns}^2 in the unit of cm^2/s. The line labeled 0 is what one would expect if heat and rotation-induced vortices were independent.

(3) *State* $V_{c1}<V_{ns}<V_{c2}$. Because of the lack of direct flow visualization in helium II, the nature of the flow past the instability ($V_{ns}>V_{c1}$) was a mystery to Swanson *et al.*[17]

(4) *Transition* $V_{ns}=V_{c2}$. The existence of a second critical velocity V_{c2} was unexpected. The nature of the transition at $V_{ns}=V_{c2}$ was not clear to Swanson *et al.*

(5) *State* $V_{ns}>V_{c2}$. What kind of flow exists in the third region ($V_{ns}>V_{c2}$) was a mystery too.

(6) *Missing vortex line density*. Swanson *et al.* found that the rotation added fewer than the expected $L_R=2\Omega/\kappa$ vortex lines to those made by the counterflow current, $L_H=\gamma_H^2 V_{ns}^2$. This means that the observed vortex line density in the presence of heat flow and rotation was less than the expected value L_R+L_H. The effect is particularly evident at high values of V_{ns} as shown in Fig. 4, where the excess line density with rotation $L-L_H$ is shown versus Ω at different values of V_{ns} up to the highest value which was applied.

IV. VORTEX DYNAMICS IN A ROTATING FRAME

The vortex filament model is very useful to study the motion of superfluid ^{4}He because the vortex core radius $a_0 \sim 10^{-8}$ cm is microscopic, hence much smaller than any flow scales of interest. Moreover, unlike what happens in classical fluid dynamics, the circulation $\kappa=9.97\times 10^{-4}$ cm^2/s is fixed by quantum constraint, which simplifies the model even further.

Helmholtz's theorem for a perfect fluid states that a vortex moves with self-induced velocity produced by the shape of the vortex itself. Therefore the velocity $\dot{\mathbf{s}}_0$ of a vortex filament at the point $\mathbf{s}$ in the absence of mutual friction is governed by the Biot-Savart law and can be expressed as[18]

$$\dot{\boldsymbol{s}}_0=\frac{\kappa}{4\pi}\boldsymbol{s}'\times\boldsymbol{s}''\ln\left(\frac{2(l_+l_-)^{1/2}}{e^{1/4}a_0}\right)+\frac{\kappa}{4\pi}\int'\frac{(\boldsymbol{s}_1-\boldsymbol{r})\times d\boldsymbol{s}_1}{|\boldsymbol{s}_1-\boldsymbol{r}|^3}. \tag{4}$$

Here the vortex filament is represented by the parametric equation $\boldsymbol{s}=\boldsymbol{s}(\xi,t)$. The first term means the localized-induction velocity, where the symbols l_+ and l_- are the lengths of the two line elements which are adjacent to a given point after discretization of the filament, and the prime denotes differentiation of $\boldsymbol{s}$ with respect to the arclength ξ. The second term represents the nonlocal field by carrying out the integral along the rest of the filament on which $\boldsymbol{s}_1$ refers to a point.

If the temperature is finite, the normal-fluid fraction is nonzero and its effects must be taken into account. The normal fluid induces a mutual friction force which drags the vortex core of a superfluid vortex filament for which the velocity of point $\boldsymbol{s}$ is given by

$$\dot{\boldsymbol{s}}=\dot{\boldsymbol{s}}_0+\alpha\boldsymbol{s}'\times(\boldsymbol{v}_{\rm ns}-\dot{\boldsymbol{s}}_0)-\alpha'\boldsymbol{s}'\times[\boldsymbol{s}'\times(\boldsymbol{v}_{\rm ns}-\dot{\boldsymbol{s}}_0)], \tag{5}$$

where α and α' are known temperature-dependent friction coefficients and $\dot{\boldsymbol{s}}_0$ is calculated from Eq. (4). More details of the numerical method and of how it is implemented are described in Ref. 23.

In order to make progress in our problem, we need to generalize this vortex dynamics approach to a rotating frame[24]. The natural way to perform the calculation in a rotating frame would require to consider a cylindrical container. We do not follow this approach for two reasons. First, our formulation is implemented using the full Biot-Savart law, not the localized-induction approximation often used in the literature. This would require to place image vortices beyond the solid boundary to impose the condition of no flow across it. This has been done in Cartesian (cubic) geometry, but it is difficult to implement in cylindrical geometry. Second, the original experiment by Swanson *et al.*[17] was carried out in a rotating channel with a square cross section.

In a rotating vessel the equation of motion of vortices is modified by two effects. The first is the force acting upon the vortex due to the rotation. According to the Helmholtz's theorem, the generalized force acting upon the vortex is balanced by the Magnus force:

$$\rho_s\kappa(\boldsymbol{s}'\times\dot{\boldsymbol{s}}_0)=\frac{\delta F'}{\delta\boldsymbol{s}}, \tag{6}$$

where $F'=F-\boldsymbol{\Omega}\cdot\boldsymbol{M}$ is the free energy of a system in a frame rotating around a fixed axis with the angular velocity $\boldsymbol{\Omega}$ and the angular momentum $\boldsymbol{M}$. Taking the vector product of Eq. (6) with $\boldsymbol{s}'$, we obtain the velocity $\dot{\boldsymbol{s}}_0$. The first term F due to the kinetic energy of vortices gives Biot-Savart law and the second term $\boldsymbol{\Omega}\cdot\boldsymbol{M}$ leads to the velocity $\dot{\boldsymbol{s}}_{\rm rot}$ of the vortex caused by the rotation:

$$\begin{aligned}\dot{\boldsymbol{s}}_{\rm rot}=\frac{1}{4\pi}\int\Bigg\{&3\frac{\boldsymbol{s}'\times\boldsymbol{R}}{|\boldsymbol{R}|^5}[(\boldsymbol{\Omega}\cdot\boldsymbol{s}')(\boldsymbol{r}\cdot\boldsymbol{R})-(\boldsymbol{\Omega}\cdot\boldsymbol{R})(\boldsymbol{r}\cdot\boldsymbol{s}')]\\&+\frac{\boldsymbol{s}'\times\boldsymbol{\Omega}}{|\boldsymbol{R}|^5}[|\boldsymbol{R}|^2(\boldsymbol{r}\cdot\boldsymbol{s}')-3(\boldsymbol{r}\cdot\boldsymbol{R})\ \ (\boldsymbol{R}\cdot\boldsymbol{s}')]\\&-\frac{\boldsymbol{s}'\times\boldsymbol{r}}{|\boldsymbol{R}|^5}[|\boldsymbol{R}|^2(\boldsymbol{\Omega}\cdot\boldsymbol{s}')-3(\boldsymbol{\Omega}\cdot\boldsymbol{R})(\boldsymbol{R}\cdot\boldsymbol{s}')]-\frac{\boldsymbol{\Omega}\times\boldsymbol{r}}{|\boldsymbol{R}|^3}\\&+\frac{\boldsymbol{s}'\cdot(\boldsymbol{\Omega}\times\boldsymbol{r})}{|\boldsymbol{R}|^3}\boldsymbol{s}'\Bigg\}d\boldsymbol{r},\end{aligned} \tag{7}$$

with $\boldsymbol{R}=\boldsymbol{r}-\boldsymbol{s}$. The second effect is the superflow induced by the rotating vessel. For a perfect fluid we know the analytical solution of the velocity inside a cube of size D rotating with the angular velocity $\boldsymbol{\Omega}=\Omega\hat{\boldsymbol{z}}$:[25]

$$\begin{aligned}\boldsymbol{v}_{{\rm cub},x}=\frac{8\Omega}{\pi^2}\sum_{n=0}^{\infty}\frac{(-1)^n}{(2n+1)^2}\frac{D}{2}{\rm sech}\frac{(2n+1)\pi}{2}\\\times[\sinh Y\cos X-\cosh X\sin Y]\end{aligned} \tag{8}$$

$$\begin{aligned}\boldsymbol{v}_{{\rm cub},y}=\frac{8\Omega}{\pi^2}\sum_{n=0}^{\infty}\frac{(-1)^n}{(2n+1)^2}\frac{D}{2}{\rm sech}\frac{(2n+1)\pi}{2}\\\times[\cosh Y\sin X-\sinh X\cos Y],\end{aligned} \tag{9}$$

with $X=(2n+1)\pi x/D$ and $Y=(2n+1)\pi Y/D$. In a rotating frame these terms are added to the velocity $\dot{\boldsymbol{s}}_0$ without the mutual friction, so Eq. (4) is replaced by

$$\begin{aligned}\dot{\boldsymbol{s}}_0=\frac{\kappa}{4\pi}\boldsymbol{s}'\times\boldsymbol{s}''\ln\left(\frac{2(l_+l_-)^{1/2}}{e^{1/4}a_0}\right)+\frac{\kappa}{4\pi}\int'\frac{(\boldsymbol{s}_1-\boldsymbol{r})\times d\boldsymbol{s}_1}{|\boldsymbol{s}_1-\boldsymbol{r}|^3}+\dot{\boldsymbol{s}}_{\rm rot}\\+\boldsymbol{v}_{\rm cub}.\end{aligned} \tag{10}$$

Some important quantities useful for characterizing the rotating tangle will be introduced. The vortex line density is

$$L=\frac{1}{\Lambda}\int d\xi, \tag{11}$$

where the integral is made along all vortices in the sample volume Λ. The polarization of the tangle may be measured by the quantity

$$\langle s_z'\rangle=\frac{1}{L\Lambda}\int d\xi\boldsymbol{s}'(\xi)\cdot\hat{\boldsymbol{z}}, \tag{12}$$

as a function of time.

The actual numerical technique used to perform the simulation has been already described.[23] Here it is enough to say that a vortex filament is represented by a single string of points at a distance $\Delta\xi$ apart. When two vortices approach within $\Delta\xi$, they are assumed to reconnect.[26] The computational sample is taken to be a cube of size $D=1.0$ cm. We adopt periodic boundary conditions along the rotating axis and rigid boundary conditions at the side walls. All calculations are made under the fully Biot-Savart law, placing image vortices beyond the solid boundaries. The space resolution is $\Delta\xi = 1.83\times10^{-2}$ cm and the time resolution is $\Delta t = 4.0\times10^{-3}$ s. All results presented in this paper refer to calculations made in the rotating frame at the temperature $T = 1.6$ K. The uniform counterflow $\boldsymbol{v}_{\rm ns}$ is applied along the z axis.

V. THE FIRST CRITICAL VELOCITY

Swanson *et al.*[17] found that the first critical velocity V_{c1} was proportional to $\Omega^{1/2}$; this functional dependence and the actual numerical values were consistent with interpreting the transition at $V_{ns} = V_{c1}$ as the DG instability of Kelvin waves. Glaberson *et al.*[5] considered an array of quantized vortices (which they modeled as a continuum) inside a container rotating at an angular velocity Ω. They found that, in the absence of friction, the dispersion relation of a Kelvin wave of wave number k is

$$\omega = 2\Omega + \nu k^2, \tag{13}$$

where ω is the angular frequency of the Kelvin wave, ν is given by

$$\nu = \frac{\kappa}{4\pi}\ln\left(\frac{b}{a_0}\right), \tag{14}$$

where $b \approx L^{-1/2}$ is the average distance between vortices.

Glaberson *et al.*[5] showed that the dispersion law (13) has a critical velocity

$$V_{DG} = (\omega/k)_{min} = 2(2\Omega\nu)^{1/2} \tag{15}$$

at the critical wave number

$$k_{DG} = \sqrt{\frac{2\Omega}{\nu}}. \tag{16}$$

If the axial flow $V_{\rm ns}$ exceeds V_{DG} for some value of k, then Kelvin waves with that wave number k (which are always present at very small amplitude due to thermal excitations and mechanical vibrations) become unstable and grow exponentially in time. Physically, the phase velocity of the mode k is equal to the axial flow, so energy is fed into the Kelvin wave by the normal flow.

Figure 5 illustrates the DG instability. The computations were performed in a periodic box of size 1 cm in a reference frame rotating with angular velocity $\Omega = 9.97\times10^{-3}$ s^{-1}, for which $V_{DG} = 0.010$ cm/s. Figure 5(a) confirms that when $V_{ns} = 0.008$ cm/s $< V_{\rm crit}$ the vortex lines remain stable. Figure 5(b) shows that, at $V_{ns} = 0.015$ cm/s $> V_{\rm crit}$, Kelvin waves become unstable and grow, as predicted. Figures 5(c–f) show that Kelvin waves of larger wave number become unstable at higher counterflow velocity.

Linear stability theory[27] can only predict two quantities: the first is the critical value of the driving parameter (V_{DG} in our case) at which a given state (the vortex array in our case) becomes unstable because infinitesimal perturbations grow rather than decay; the second is the exponential growth or decay rate of these perturbations for a given value of the driving parameter. Therefore the linear stability theory of Glaberson[5] cannot answer the question of what is the new solution which grows beyond the DG instability at $V_{ns} = V_{c1}$: to determine this new solution we must solve the governing nonlinear equations of motion, which is what we do in the following section.

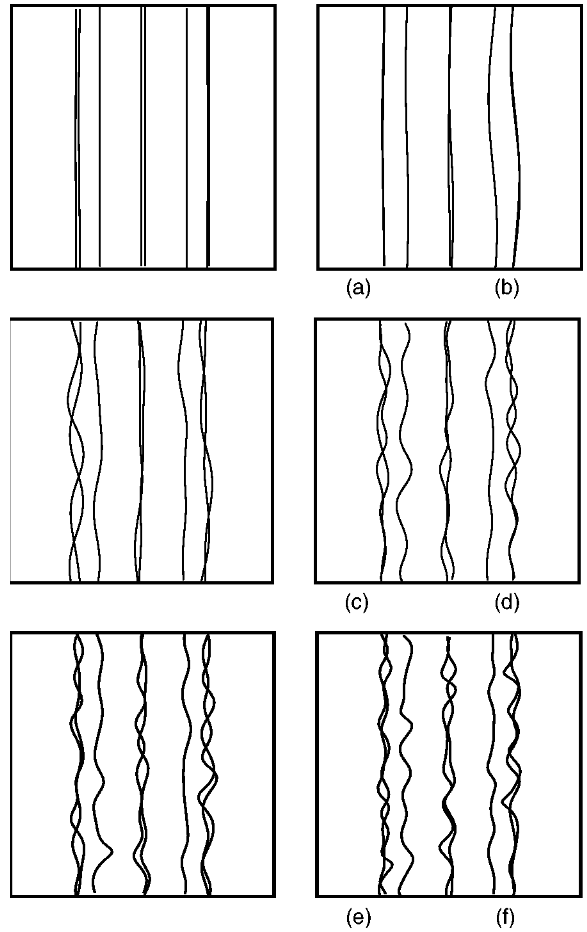

FIG. 5. Numerical simulations of the Donnelly-Glaberson instability at $\Omega = 9.97\times10^{-3}$ s^{-1} and $T = 1.6$ K. Snapshots of Kelvin wave whose amplitude grows exponentially with time driven by the following counterflow velocities V_{ns}: (a) $V_{ns} = 0.008$ cm/s, (b) $V_{ns} = 0.015$ cm/s, (c) $V_{ns} = 0.03$ cm/s, (d) $V_{ns} = 0.05$ cm/s, (e) $V_{ns} = 0.06$ cm/s, (f) $V_{ns} = 0.08$ cm/s.

VI. THE REGION ABOVE THE FIRST CRITICAL VELOCITY

Because of the computational cost of the Biot-Savart law, it is not practically possible to compute vortex tangle with densities which are as high $[L = O(10^4)$ cm$^{-2}]$ as those achieved in the experiment. Nevertheless, numerical simulations performed at smaller, computationally realistic values of L are sufficient to shed light into the physical processes involved. Some results which we describe have been already presented in preliminary form;[16] together with more recent computer simulations, the picture which emerges and which we present here gives a good understanding of the experimental findings of Swanson *et al.*,[17] at least as far as the

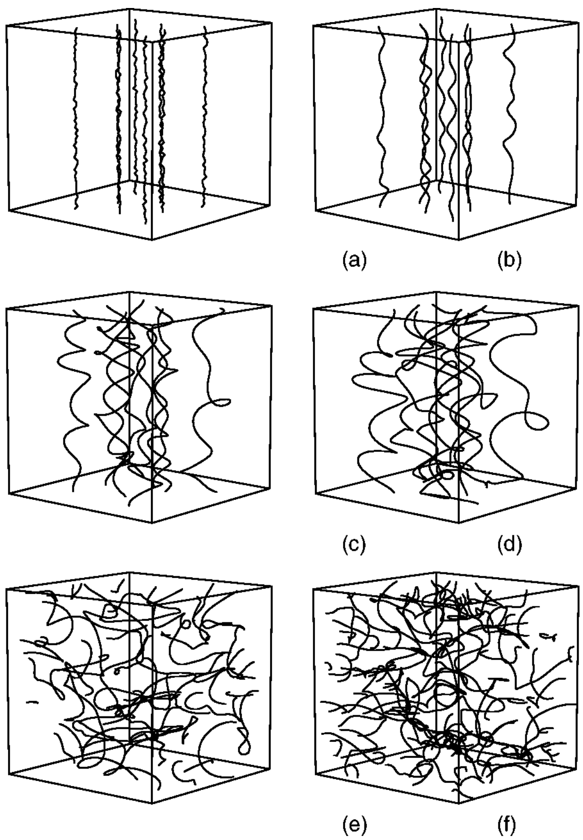

FIG. 6. Numerical simulation of rotating turbulence at $T=1.6$ K, $\Omega=9.97\times10^{-3}$ s^{-1}, and $V_{ns}=0.08$ cm/s. Computed vortex tangle at the following times: (a) $t=0$ s, (b) $t=16$ s, (c) $t=28$ s, (d) $t=36$ s, (e) $t=80$ s, (f) $t=600$ s.

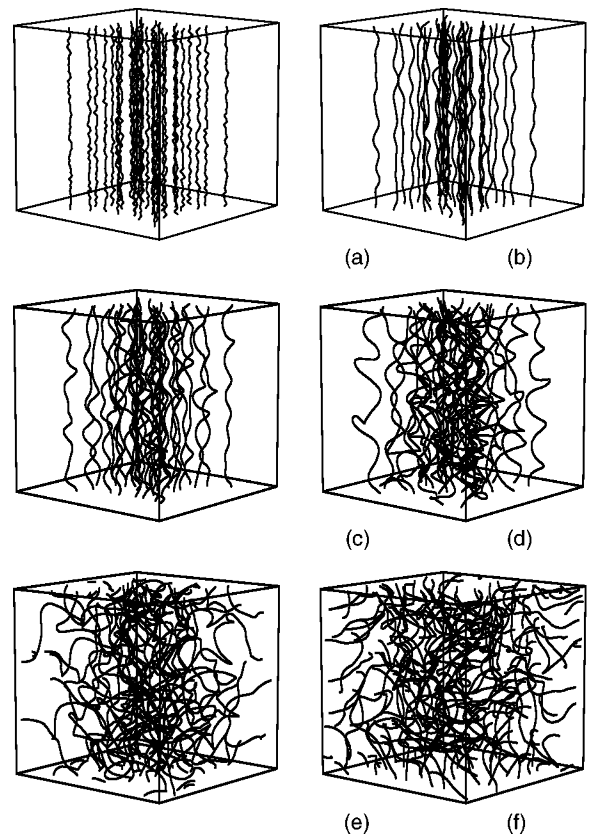

FIG. 7. Numerical simulation of rotating turbulence at $T=1.6$ K, $\Omega=4.98\times10^{-2}$ s^{-1}, and $V_{ns}=0.08$ cm/s. Computed vortex tangle at the following times: (a) $t=0$ s, (b) $t=12$ s, (c) $t=20$ s, (d) $t=28$ s, (e) $t=40$ s, (f) $t=160$ s.

transition at $V_{ns}=V_{c1}$ and the flow in the region $V_{c1}<V_{ns}<V_{c2}$ are concerned.

The time sequence contained in Fig. 6 illustrates the evolution of a vortex array at a relatively small angular velocity, $\Omega=9.97\times10^{-3}$ s^{-1}, in the presence of the counterflow $V_{ns}=0.08$ cm/s. Figure 6(a) shows the initial $N=8$ parallel vortex lines at $t=0$. This initial vortex configuration corresponds to a vortex line density which is somewhat less than the equilibrium value given by Eq. (1). This is not a problem because Eq. (1) only refers to an infinite system. Equation (1) can be applied to the experiment of Swanson *et al.* because their values of Ω are large. In our numerical simulation the rotation rate Ω (hence L) is small; we thus expect that the geometry (flow in a square container) and the presence of the walls are important[28] so Eq. (1) is only an approximation. The best way to proceed is thus to let a given vortex configuration to relax into a local free-energy minimum by direct time stepping, so that it becomes steady in the rotating frame of reference. The vortices have been seeded with small random perturbations to make the simulation more realistic. The absence of these perturbations would make the phase of the Kelvin waves synchronize on all vortices to delay reconnections. As the evolution proceeds, perturbations with high wave numbers are damped by friction, whereas perturbations which are linearly DG unstable grow exponentially, hence Kelvin waves become visible [Fig. 6(b)]. When the amplitude of the Kelvin waves becomes of the order of the average vortex separation, reconnections take place [Fig. 6(c)] starting from time $t=31.456$ s. The resulting vortex loops disturb the initial vortex array, leading to an apparently random vortex tangle [Fig. 6(d)]. After the initial exponential growth (which is predicted by the theory of the DG instability), nonlinear effects (vortex interactions and vortex reconnections) become important and nonlinear saturation takes place.

Figure 7 shows a similar time sequence at the same counterflow velocity $V_{ns}=0.8$ cm/s but at higher rotation rate, $\Omega=4.98\times10^{-2}$ s^{-1}. In this case we have $N=33$ initial parallel vortices [Fig. 7(a)]. At $t=12$ s [Fig. 7(b)] it is still $N=33$. Then the amplitude of the Kelvin waves becomes so large that, starting at $t=21.336$ s (earlier than in the previous calculation, as expected), lots of reconnections take place and N increases; for example, we have $N=83$ at $t=160$ s [Fig. 7(f)].

It is instructive to compare these results with ordinary counterflow in the absence of rotation. Figure 8 shows a vortex tangle obtained for $\Omega=0$ and $V_{ns}=0.08$ cm/s. The dynamics starts from $N=6$ vortex rings. It has been known since the early work of Schwarz[18] that the resulting tangle does not depend on the initial condition. In this particular simulation the vortices develop to a turbulent tangle.

Figure 9 shows that in all three cases (small rotation, large

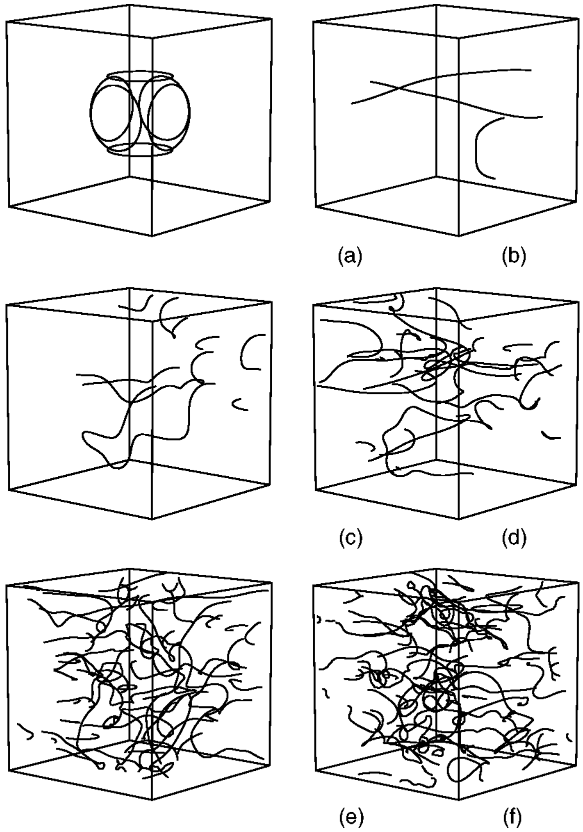

FIG. 8. Numerical simulation of counterflow turbulence at $T = 1.6$ K in the absence of rotation ($\Omega = 0$) for $V_{ns} = 0.08$ cm/s. Computed vortex tangle at the following times: (a) $t = 0$ s, (b) $t = 120$ s, (c) $t = 360$ s, (d) $t = 520$ s, (e) $t = 680$ s, (f) $t = 1160$ s.

rotation, no rotation) the vortices, after an initial transient, saturate to a statistically steady, turbulent state, which is characterized by a certain average value of L. In the case of $\Omega \neq 0$ [Figs. 9(a) and 9(b)], it is apparent that the initial growth is exponential, which confirms the occurrence of a linear instability.

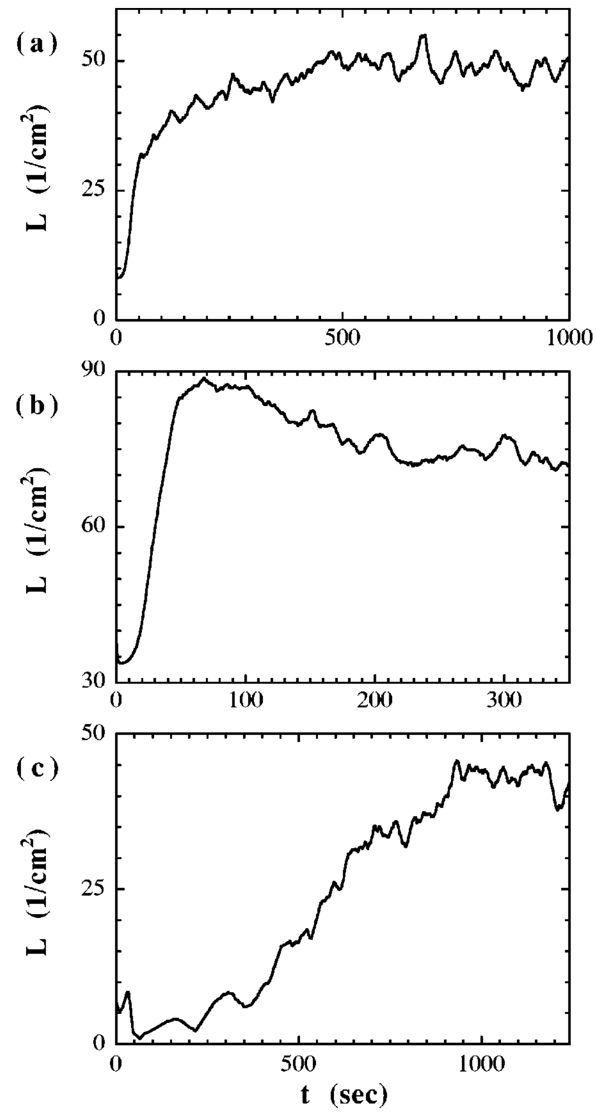

FIG. 9. Vortex line density L vs time t at $T = 1.6$ K and $V_{ns} = 0.08$ cm/s for (a) $\Omega = 9.97 \times 10^{-3}$ s^{-1}, (b) $\Omega = 4.98 \times 10^{-2}$ s^{-1}, (c) $\Omega = 0$ s^{-1}.

VII. POLARIZED TURBULENCE

Looking carefully at the saturated tangle at higher rotation in Fig. 7(f) we notice that there are more loops oriented vertically than horizontally. The effect is not visible at lower rotation in Fig. 6(f) and at zero rotation in Fig. 8(f). The degree of polarization of the tangle is represented by $\langle s_z' \rangle$ of Eq. (10). This quantity captures the difference between a vortex array (for which $\langle s_z' \rangle = 1$ because all lines are aligned in the $+z$ direction) and a random vortex tangle (for which $\langle s_z' \rangle = 0$ because there is an equal amount of vorticity in the $+z$ and $-z$ directions). Figure 10 shows how $\langle s_z' \rangle$ changes with time in the three cases (small rotation, large rotation, no rotation) considered. The quantities of interest are the values of $\langle s_z' \rangle$ at large times in the saturated regimes. In the absence of rotation [Fig. 10(c)] $\langle s_z' \rangle$ is negligible but not exactly zero ($\langle s_z' \rangle \approx 0.01$), certainly because the driving counterflow is along the z direction. This small anisotropy of the counterflow tangle has been already reported in the literature.[30] At small rotation in Fig. 10(a) there is a small but finite polarization $\langle s_z' \rangle \approx 0.15$, whereas at higher rotation the polarization is significant ($\langle s_z' \rangle \approx 0.45$)—in fact it is even visible with the naked eye in Fig. 7(f).

Figure 11 shows the quantity $\langle s_z' \rangle L$ as a function of time. It is apparent that this quantity, which represents the average vorticity in the direction of rotation, remains approximately constant during the time evolution. This means that the (disordered) tangle has approximately the same ''rotation'' as the initial (ordered) vortex lattice. This effect answers directly the simple question raised by Swanson *et al.*, as to why L_R and L_H do not simply add together.

Figure 12 shows the calculated dependence of the vortex line density L on the counterflow velocity V_{ns} at different rotation rates Ω. The figure shows a dependence of L on V_{ns} which is similar to Fig. 3. The only difference is that the scale of the axes in the paper by Swanson *et al.* is bigger—in this particular figure they report vortex line densities as high

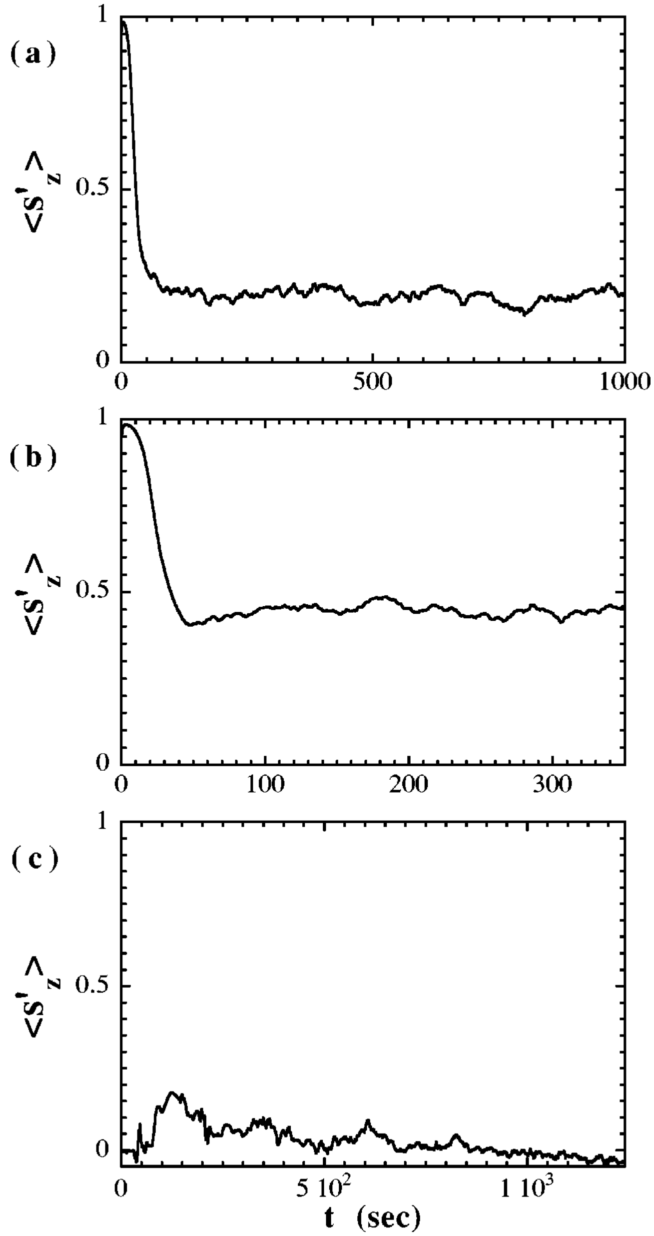

FIG. 10. Tangle's polarization $\langle s_z' \rangle$ vs time t at $T=1.6$ K and $V_{ns}=0.08$ cm/s for (a) $\Omega=9.97\times10^{-3}$ s^{-1}, (b) $\Omega=4.98\times10^{-2}$ s^{-1}, (c) $\Omega=0$ s^{-1}.

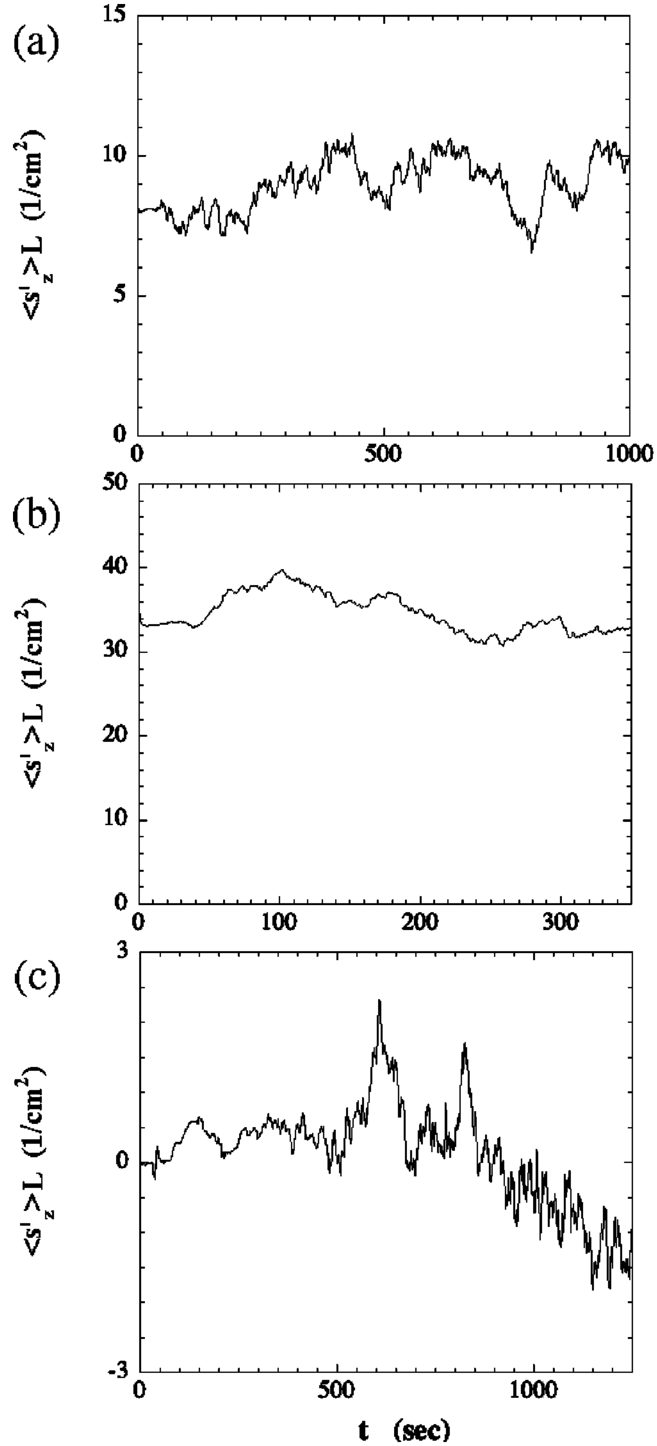

FIG. 11. Product $\langle s_z' \rangle L$ vs time t at $T=1.6$ K and $V_{ns}=0.08$ cm/s for (a) $\Omega=9.97\times10^{-3}$ s^{-1}, (b) $\Omega=4.98\times10^{-2}$ s^{-1}, (c) $\Omega=0$ s^{-1}.

as $L\approx2500$ cm^{-2}, whereas our calculations are limited to $L\approx80$ cm^{-2}. Despite the lack of overlap between the experimental and numerical ranges, there is clear qualitative similarity between the figures. It is apparent that the critical velocity beyond which L increases with V_{ns} is much reduced by the presence of rotation, which is consistent with the experiment.

Figure 13 shows the calculated polarization $\langle s_z' \rangle$ as a function of counterflow velocity V_{ns} at different rotation rates Ω. It is apparent that the polarization decreases with the counterflow velocity and increases with the rotation, which shows the competition between order induced by rotation and disorder induced by flow.

We conclude that the nonlinear saturated state which takes place beyond the DG instability in the region $V_{c1}<V_{ns}<V_{c2}$ and which was observed by Swanson *et al.*[17] is a state of *polarized turbulence*.

It is known[18] that the dynamics of superfluid turbulence is determined by two main effects—mutual friction and vortex reconnection—thus it is interesting to analyze their roles in polarized turbulence. First we consider the friction. Follow-

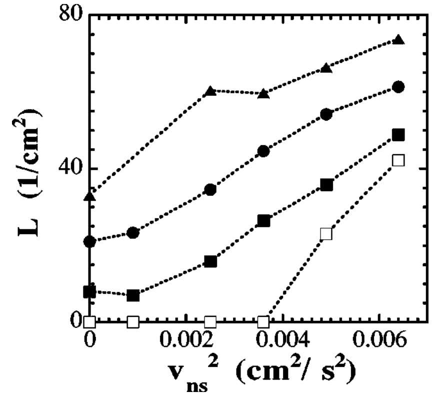

FIG. 12. Vortex line density L vs V_{ns}^2 at $T=1.6$ K for $\Omega=0$ (write circle), $\Omega=9.97\times10^{-3}$ s^{-1} (black circle), $\Omega=2.99\times10^{-2}$ s^{-1} (triangle), and $\Omega=4.98\times10^{-2}$ s^{-1} (square). The dotted lines are guides to the eye. The error bars should be estimated from the fluctuations around the statistical steady state which are about 10%.

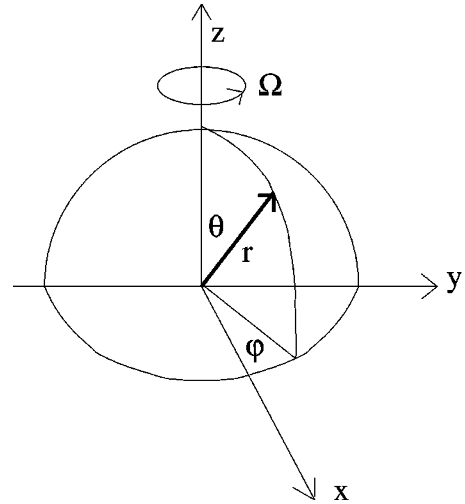

FIG. 14. Vortex segment in the presence of rotation.

ing Ref. 12, we use the following idealized model of the action of friction: consider a straight vortex segment in the presence of normal-fluid rotation as in Fig. 14. Using spherical coordinates (r,θ,ϕ), we have $\mathbf{s}'=(1,0,0)$ and $\boldsymbol{v}_{ns}=(0,0,\Omega r\sin\theta)$. Since there is no self-induced velocity, from Eq. (5) we find that the components of the velocity of the segment, $\dot{\mathbf{s}}=(dr/dt, r d\theta/dt, r\sin\theta d\phi/dt)$, are given by $dr/dt=0$, $d\theta/dt=-\alpha\Omega\sin\theta$, and $d\phi/dt=\alpha'\Omega$. The solution of these equations is that r remains constant, $\phi=\alpha'\Omega t+\phi_0$ and

$$\theta=2\tan^{-1}[\tan(\theta_0/2)(e^{-\alpha\Omega t})], \tag{17}$$

where ϕ_0 and θ_0 are the initial angles. Note that $\theta\rightarrow0$ for $t\rightarrow\infty$. In conclusion the vortex segment is advected in the azimuthal direction by the normal fluid and rotates upward, aligning itself with the direction of rotation of the vessel. The azimuthal motion is small because α' is typically smaller than α, whereas the motion in the meridional direction θ is

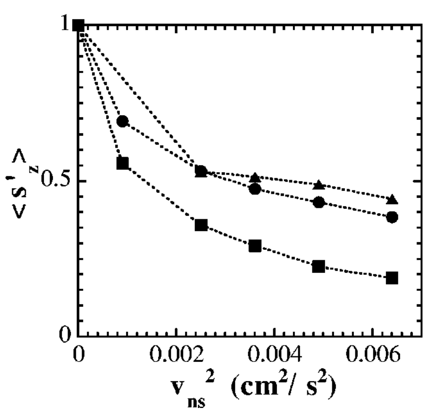

FIG. 13. Tangle's polarization $\langle s_z'\rangle$ vs V_{ns}^2 at $T=1.6$ K for $\Omega=9.97\times10^{-3}$ s^{-1} (circle), $\Omega=2.99\times10^{-2}$ s^{-1} (triangle), and $\Omega=4.98\times10^{-2}$ s^{-1} (square). The dotted lines are guides to the eye. The error bars, again estimated from the fluctuations, are about 20%.

significant and explains the observed polarization. If the vortex is not straight, there is also the competing effect of the self-induced motion in the direction of the binormal that is induced by the local curvature. The isolated vortex segment model predicts also that, if we continue the calculation but set the counterflow velocity equal to zero, the recovery of the polarized lattice takes place with time scale $1/(\alpha\Omega)$. For $\Omega=9.97\times10^{-3}$ s^{-1} this corresponds to 1000 s. We made the numerical simulation of the vortex tangle in the same situation to find the time scale 600 s, which agrees with the above simple estimation; the difference is clearly due to vortex interaction and reconnections.

Second we consider vortex reconnections. Reconnections tend to randomize the geometry of the vortex configuration. For example, consider the first vortex reconnection. The event creates vortex cusps which form large amplitude Kelvin waves.[31] Since these waves extend in the direction perpendicular to the plane that contained the initial vortices, the probability of another reconnection with neighboring vortices increases. The vortex reconnection rate f (number of vortex reconnections per unit time per unit volume) has been the subject of recent investigations:[23,32] it is found that the reconnection rate obeys the scaling law $f\sim L^{5/2}$. Is that still true in the case of polarized turbulence? Table I shows that at increasing rotating rates Ω the ratio $f/L^{5/2}$ decreases. Although we do not have enough data to determine what should be the exact scaling of f with respect to L as a function of Ω, the result suggests that, as the tangle becomes more polarized, there is less vortex length in the x-y plane, hence there are less vortex reconnections.

TABLE I. Vortex reconnections.

Ω (rad/s)	L(cm^{-2})	f(s^{-1} cm^{-3})	$f/L^{5/2}$ (cm^2/s)
0	43.3	5.41	4.4×10^{-4}
9.97×10^{-3}	48.7	7.20	4.3×10^{-4}
4.98×10^{-2}	74.0	16.17	3.4×10^{-4}

VIII. THE SECOND CRITICAL VELOCITY

The experiment of Swanson *et al.* shows that, at higher velocities V_{ns}, the dependence of the observed vortex line density L on V_{ns} abruptly changes at a second critical velocity V_{c2} (see Fig. 2), indicating the onset of a different state. Unfortunately we cannot explore numerically this region of parameter space at high values of V_{ns} relevant to the experiment, due to the larger vortex line densities involved. To explain the experiment we propose a qualitative theory for the second critical velocity: we argue that for $V_{ns}>V_{c2}$ the vortex tangle undergoes so many reconnections that it becomes unpolarized.

We picture the polarized vortex tangle as consisting of an ordered vortex array plus a number of perturbing vortex loops. Let τ_1 be the characteristic time scale of the growing Kelvin waves, which are induced on the vortex array by the DG instability. Let τ_2 be the typical lifetime of the vortex loops, which is determined by the friction with the normal fluid and by the relative orientation with respect to the counterflow. If $\tau_2<\tau_1$ then, although vortex loops are continually created, they do not overcome the vortex array and the total configuration retains an amount of polarization. If $\tau_2>\tau_1$ then the vortex loops do not have enough time to shrink significantly before more loops are introduced by vortex reconnections induced by growing Kelvin waves. This means that randomness is introduced by vortex reconnections at a rate which is faster than the rate at which loops disappear by friction. In conclusion, we expect that if $\tau_2>\tau_1$ the vortex configuration will be random (unpolarized).

According to this qualitative "cartoon," the order of magnitude of the critical velocity V_{c2} is given by the condition

$$\tau_1=\tau_2. \tag{18}$$

First we estimate τ_1 using a simple model. For the sake of simplicity we assume an isolated vortex line of helical shape $\boldsymbol{s}=(\epsilon\cos\phi,\epsilon\sin\phi,z)$, where $\phi=kz-\omega t$ and $\epsilon\ll 1$, hence $z\approx\xi$ is the arclength. The tangent unit vector is $\boldsymbol{s}'=d\boldsymbol{s}/d\xi\approx d\boldsymbol{s}/dz=(-k\epsilon\sin\phi,k\epsilon\cos\phi,1)$, and $\boldsymbol{s}''=(-k^2\epsilon\cos\phi,-k^2\epsilon\sin\phi,0)$. Using the local induction approximation, the self-induced velocity of the line at the point $\boldsymbol{s}$ is given by

$$\boldsymbol{v}_i=\nu'\boldsymbol{s}'\times\boldsymbol{s}'', \tag{19}$$

where $\nu'=\kappa\mathcal{L}_1/(4\pi)$ and the slowly varying term $\mathcal{L}_1=\ln[1/(ka_0)]$ is assumed constant. Neglecting higher-order terms in ϵ we have $\boldsymbol{v}_i=\nu' k^2\epsilon(\sin\phi,-\cos\phi,0)$.

In the absence of friction the equation of motion is simply $\dot{\boldsymbol{s}}=d\boldsymbol{s}/dt=\boldsymbol{v}_i$, hence, assuming that ϵ is constant, we find that the Kelvin wave oscillates with angular frequency $\omega=\nu' k^2$. This result differs from Glaberson's equation (13) because we perturbed a single-vortex line rather than a continuum of vorticity 2Ω described by the Hall-Vinen equations in the rotating frame (hence the presence of a different upper cutoff which makes ν' different from ν and the contribution 2Ω to ω).

In the presence of friction, neglecting the small mutual friction coefficient α' for simplicity, the equation of motion is $d\boldsymbol{s}/dt=\boldsymbol{v}_i+\alpha\boldsymbol{s}'\times(\boldsymbol{v}_{ns}-\boldsymbol{v}_i)$. Assuming $\boldsymbol{v}_{ns}=(0,0,V_{ns})$ and $\epsilon=\epsilon(t)$, we find that $d\epsilon/dt=\alpha(kV_{ns}-\nu' k^2)\epsilon$ hence $\epsilon(t)=\epsilon(0)\exp(\sigma t)$ where the growth rate is $\sigma=\alpha(kV_{ns}-\nu' k^2)$. Given V_{ns}, the largest growth rate occurs for $k=V_{ns}/(2\nu')$ and takes $\sigma=\alpha V_{ns}^2/(4\nu')$, for which we conclude that

$$\tau_1=\frac{1}{\sigma}=\frac{4\nu'}{\alpha V_{ns}^2}. \tag{20}$$

To estimate τ_2 we approximate the vortex loops as vortex rings of radius approximately determined by the average vortex spacing $\delta\approx L^{-1/2}$. The characteristic lifetime of a ring of radius R in the presence of friction is[29]

$$\tau_2=\frac{2\rho_s\pi R^2}{\gamma\mathcal{L}_2}, \tag{21}$$

where $\mathcal{L}_2=\ln[(8R/a_0)-1/2]$ and γ is a known friction coefficient.[29] Setting $2R=\delta=L^{-1/2}$ and using Eq. (18), we conclude that the polarized tangle is unstable if

$$L<C_2V_{ns}^2, \tag{22}$$

where

$$C_2=\frac{\alpha\pi^2\rho_s}{2\gamma\Gamma\mathcal{L}_1\mathcal{L}_2} \tag{23}$$

Equation (22) has the same dependence of L on V_{ns} as that observed experimentally. At $T=1.65$ K we have[29] $\rho_s=0.1168$ g/cm^3, $\gamma=1.3\times10^{-5}$ g/cm s, $\alpha=0.11$. Since $a_0\approx10^{-8}$ cm and the slowly varying logarithm terms are $\approx\mathcal{L}_1\approx\mathcal{L}_2\approx10$, we conclude that $C_2\approx5\times10^4$ cm^{-4} s^2, which is of the same order of magnitude of the value $C_2=16\times10^4$ cm^{-4} s^2 found by Swanson *et al.*[17] Given the very idealized model used, the agreement is remarkable.

IX. ANALOGY WITH PARAMAGNETISM

Figure 4 shows that if the counterflow channel is rotated, the increase of vortex line density L observed by Swanson *et al.* is always *less* than what would be necessary to achieve the value $L_{\rm expt}=L_H+L_R$, which one would (naively) expect if the two effects of heat flow and rotation combined together independently. Figure 4 shows that the amount of vortex line density which is missing increases with V_{ns}. How to explain Fig. 4? It is apparent from the previous discussions that the application of the counterflow V_{ns} tends to increase the disorder of the vortex configuration by creating instability and vortex reconnections which randomize the orientation of the vortices. To the contrary, the application of the rotation Ω tends to order the vortex configuration by the polarization mechanism arising from the friction force [see Eq. (14)]. This observation suggests the following analogy between our problem (thermal counterflow in the presence of rotation) and the problem of a system of spins in a heat bath in the presence of an applied magnetic field.

Consider N spins of dipole moment μ, which are contained in a heat bath of volume V and temperature T and which are free to take any orientation in space. If we apply

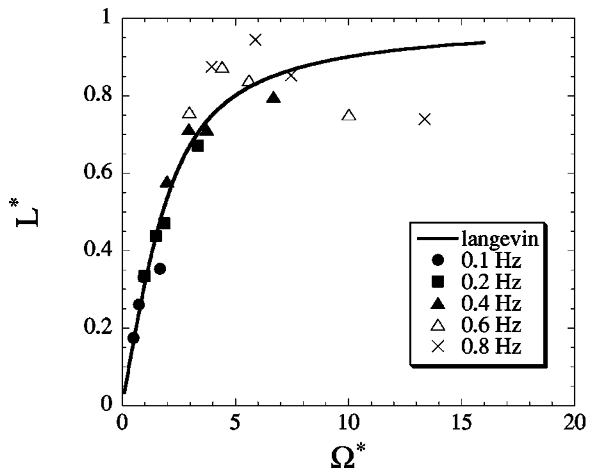

FIG. 15. Plot of $L^* = (L_{\mathrm{expt}} - L)/(bL_H)$ vs $\Omega^* = aL_R/L_H$. The solid line is the Langevin curve $f(aL_R/L_H)$.

an external magnetic field H, the resulting magnetization per unit volume is

$$M = M_{sat}\, f\left(\frac{\mu H}{k_B T}\right), \tag{24}$$

where

$$f(x) = \coth(x) - \frac{1}{x}, \tag{25}$$

is the Langevin function of argument x, k_B is Boltzmann's constant, and $M_{sat} = N\ \mu/V$.

Pursuing the analogy, we can think of the vortex tangle as a collection of "vortex segments." The segments are free to assume any orientation in space, tend to be aligned by the applied rotation Ω, and tend to be randomized by the applied counterflow V_{ns}. Hence, in analogy with the system of spins, we expect that the fractional alignment of the tangle is given by the Langevin function

$$f\left(a\,\frac{(2\Omega/\kappa)}{(\gamma_H^2 V_{ns}^2)}\right) = f(\Omega^*), \tag{26}$$

where the dimensionless quantities Ω^* and L^* are

$$\Omega^* = a\,\frac{L_R}{L_H} = a\,\frac{2\Omega}{\kappa \gamma_H^2 V_{ns}^2}, \tag{27}$$

$$L^* = \frac{L_{\mathrm{expt}} - L}{bL_H}, \tag{28}$$

and a and b are fitting parameters. Figure 15 confirms then the data of Fig. 4, when plotted in terms of Ω^* and L^*, almost collapse onto a single curve. The quantity L^* represents the relative deviation from the expected line density, that is to say L^* measures the polarization (fractional alignment) of the tangle. The fitting parameters which we have used are $a = 11$ and $b = 0.23$, whereas $\gamma_H = 98.2$ s/cm^2 is obtained from the measured vortex line density in the absence of rotation. The fact that $b < 1$ suggests that the quantity $1 - b$ can be interpreted as the effective fraction of closed vortex loops, because any vortex line ending on itself cannot produce a net rotation (rotation is due to the net number of vortex lines through a given cross section).

X. CONCLUSIONS

In conclusion, we have studied the stability of a superfluid vortex array in the presence of an applied counterflow, giving answers to some questions which were first asked by the pioneering experiment of Swanson *et al.*[17] After investigating the DG instability, V_{c1}, we have determined the existence of a state of superfluid turbulence (polarized turbulence) which is characterized by two statistically steady-state properties, the vortex line density, and the degree of polarization. Although our computed range of vortex line densities does not overlap with the much higher values obtained in the experiment, we find the same qualitative dependence of vortex line density versus counterflow velocity at different rotations. We have also made some qualitative progress to understand what happens at $V_{ns} = V_{c2}$. Although more quantitatively results are still needed to make direct contact with the experiment, the scenario which we proposed is the following: at small enough velocity $V < V_{c1}$ the axial flow cannot destabilize the ordered vortex array configuration; at $V_{ns} = V_{c1}$ the DG instability disrupts the vortex array; in the region $V_{c1} < V_{ns} < V_{c2}$ we have a state of turbulence which retains some order in the form of polarization; finally, at $V_{ns} = V_{c2}$, there are enough vortex reconnections to destroy any polarization.

Further work with more computing power will hopefully investigate other aspects of the problem, particularly what happens at high counterflow velocities and line densities. We also hope that our work will stimulate more experiments on this problem. On the theoretical side, further work will be necessary to develop a better understanding of the tangle's dynamics in terms of vortex line density as well as other measures, such as the anisotropy,[33] which describe other degrees of freedom.

It is somewhat surprising that so little is known about the destabilization of a rotational vortex array by an imposed counterflow. For example, it should be possible to observe the polarization of turbulence by using simultaneous measurements of second sound attenuation along and across the rotation axis.

Finally, our work should be of interest to other investigations of vortex arrays and how they can be destabilized in other systems, ranging from ^{3}He (Ref. 15) to atomic Bose-Einstein condensates.[34] It is also worth noticing that this study has revealed the crossover of the dimensionality of vortex systems. If one considers the three regimes in Fig. 2 one notices that, at a fixed value of V_{ns}, increasing the rotation rate makes the vortices polarized, changing the dynamics from three dimensional to two dimensional. This reduction of the dimensionality of turbulence has been observed in classical fluid mechanics.[35]

ACKNOWLEDGMENTS

The authors thank W. F. Vinen for useful discussions. C.F.B. is grateful to the Royal Society and PRARC for financially supporting this project. M.T. is grateful to Japan Society for the Promotion of Science for financially supporting this Japan-UK Scientific Cooperative Program (Joint Research Project) and through a Grant-in-Aid for scientific research (Grant No. 15340122).

[1] R.J. Donnelly, *Quantized Vortices In Helium II* (Cambridge University Press, Cambridge, England, 1991).
[2] C.F. Barenghi, R.J. Donnelly, and W.F. Vinen, *Quantized Vortex Dynamics and Superfluid Turbulence* (Springer, Berlin, 2001).
[3] A.L. Fetter, Phys. Rev. **152**, 183 (1966).
[4] D.K. Cheng, M.W. Cromar, and R.J. Donnelly, Phys. Rev. Lett. **31**, 433 (1973).
[5] W.I. Glaberson, W.W. Johnson, and R.M. Ostermeier, Phys. Rev. Lett. **33**, 1197 (1974); R.M. Ostermeier and W.I. Glaberson, J. Low Temp. Phys. **21**, 191 (1975).
[6] D.C. Samuels and D. Kivotides, Phys. Rev. Lett. **83**, 5306 (1999).
[7] S.R. Stalp, L. Skrbek, and R.J. Donnelly, Phys. Rev. Lett. **82**, 4831 (1999).
[8] J. Maurer and P. Tabeling, Europhys. Lett. **43**, 29 (1998).
[9] S.I. Davis, P.C. Hendry, and P.V.E. McClintock, Physica B **280**, 43 (2000).
[10] S.N. Fischer, A.J. Hale, A.M. Guenalt, and G.R. Pickett, Phys. Rev. Lett. **86**, 244 (2001).
[11] C.F. Barenghi, G.G. Bauer, D.C. Samuels, and R.J. Donnelly, Phys. Fluids **9**, 2631 (1997).
[12] C.F. Barenghi, S. Hulton, and D.C. Samuels, Phys. Rev. Lett. **89**, 275301 (2002).
[13] T. Araki, M. Tsubota, and S.K. Nemirowskii, Phys. Rev. Lett. **89**, 145301 (2002).
[14] W.F. Vinen, Phys. Rev. B **61**, 1410 (2000); W.F. Vinen and J.J. Niemela, J. Low Temp. Phys. **129**, 213 (2002).
[15] A.P. Finne, T. Araki, R. Blaauwgeers, V.B. Eltsov, N.B. Kopnin, M. Krusius, L. Skrbek, M. Tsubota, and G.E. Volovik, Nature (London) **424**, 1022 (2003).
[16] M. Tsubota, T. Araki, and C.F. Barenghi, Phys. Rev. Lett. **90**, 205301 (2003).
[17] C.E. Swanson, C.F. Barenghi, and R.J. Donnelly, Phys. Rev. Lett. **50**, 190 (1983).
[18] K.W. Schwarz, Phys. Rev. Lett. **49**, 283 (1982); Phys. Rev. B **31**, 5782 (1985); **38**, 2398 (1988).
[19] J.T. Tough, in *Progress in Low Temperature Physics*, edited by D.F. Brewer (North-Holland, Amsterdam, 1982), Vol. VIII, p. 134.
[20] W.F. Vinen, Proc. R. Soc. London, Ser. A **242**, 493 (1957); **243**, 400 (1958).
[21] D.J. Melotte and C.F. Barenghi, Phys. Rev. Lett. **80**, 4181 (1998).
[22] C.F. Barenghi, K. Park, and R.J. Donnelly, Phys. Lett. **84A**, 453 (1981).
[23] M. Tsubota, T. Araki, and S.K. Nemirowskii, Phys. Rev. B **62**, 11 751 (2000).
[24] M. Tsubota and H. Yoneda, J. Low Temp. Phys. **101**, 815 (1995).
[25] L.M. Milne-Thomson, *Theoretical Hydrodynamics*, 5th ed., (Macmillan, New York, 1968) p. 271.
[26] J. Koplik and H. Levine, Phys. Rev. Lett. **71**, 1375 (1993).
[27] P.G. Drazin and W.H. Reid, *Hydrodynamics Stability* (Cambridge University Press, Cambridge, England, 1981).
[28] Reduced vortex line density due to edge effects has been discussed, for example, by D. Stauffer and A.L. Fetter [Phys. Rev. **168**, 156 (1968)] and by J.A. Northby and R.J. Donnelly [Phys. Rev. Lett. **25**, 214 (1970)].
[29] C.F. Barenghi, R.J. Donnelly, and W.F. Vinen, J. Low Temp. Phys. **52**, 189 (1983).
[30] R.T. Wang, C.E. Swanson, and R.J. Donnelly, Phys. Rev. B **36**, 5240 (1987).
[31] D. Kivotides, J.C. Vassilicos, D.C. Samuels, and C.F. Barenghi, Phys. Rev. Lett. **86**, 3080 (2001).
[32] D.R. Poole, H. Scoffield, C.F. Barenghi, and D.C. Samuels, J. Low Temp. Phys. **132**, 97 (2003).
[33] T. Lipniacki, Phys. Rev. B **64**, 214516 (2001).
[34] M. Tsubota, K. Kasamatsu, and M. Ueda, Phys. Rev. A **65**, 023603 (2002).
[35] M. Hossain, Phys. Fluids **6**, 1077 (1994).